Electronic Supporting Information

Er^{3+} activated $Ba_2V_2O_7$ Upconversion Nanosheets for Dual-mode Temperature Sensing

Satish Kumar Samal, Sahana Kulkarni, Jyoti Yadav, and Boddu S. Naidu*

Energy and Environment Unit, Institute of Nanoscience and Technology (INST), Mohali, Punjab, India-140306.

**E-mail: naidu245@gmail.com, sanyasinaidu@inst.ac.in*

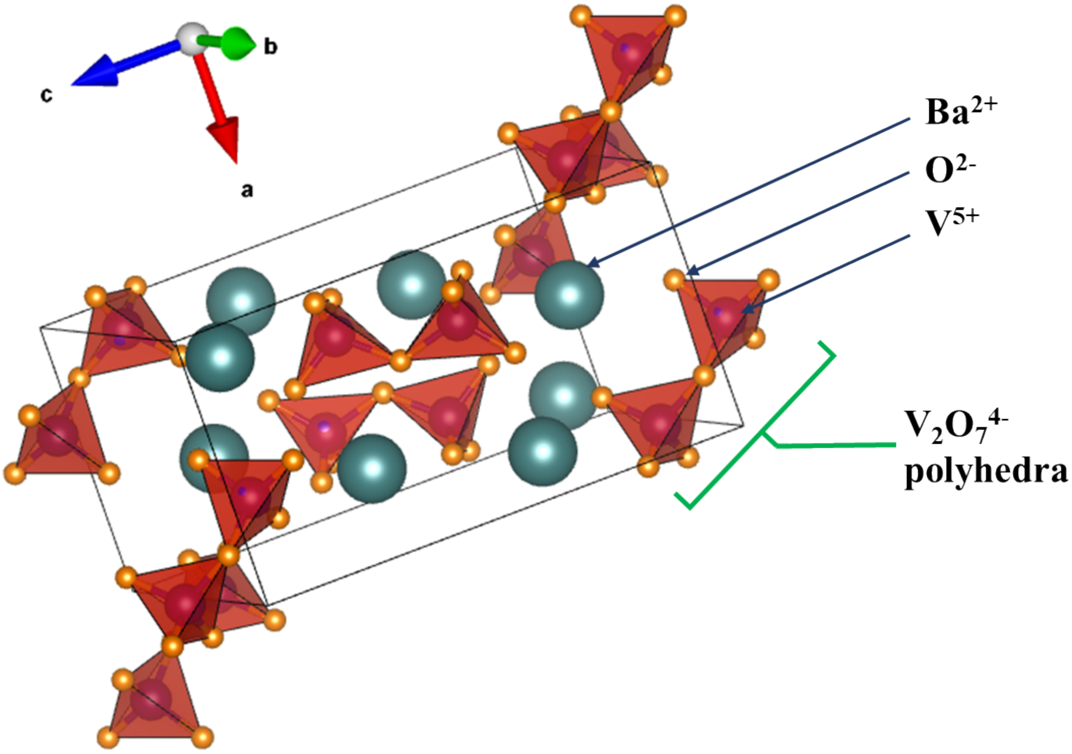

Fig. S1 Schematic of the crystal structure of $Ba_2V_2O_7$.

Figure S1 depicts the $Ba_2V_2O_7$ structure[1]. Sheets of $Ba_2V_2O_7$ form in the triclinic $P\bar{1}$ space group. Two V^{5+} ions form corner-sharing VO_4 tetrahedra to make a divanadate group. Repeated divanadate groups connected in eclipsed configuration to form sheets of divanadate. These sheets are connected through Ba^{2+} ions. There are four types of Ba^{2+} sites, viz. one with coordination number 9, two ions with coordination number 8, and the last one with 10 coordination.

Table S1: Lattice parameters of Er^{3+} doped $Ba_2V_2O_7$ phosphor.

Concentration of Er^{3+} (x)	**a(Å)**	**b(Å)**	**c(Å)**	**V(Å^3)**
0.0	7.350	7.333	13.585	721.95
0.02	7.338	7.322	13.577	719.34
0.05	7.327	7.316	13.573	717.53
0.10	7.323	7.314	13.559	716.08
0.125	7.323	7.311	13.545	715.19
0.15	7.320	7.308	13.551	714.79

The lattice parameters were calculated with UNITCELL software, and further visualization was carried out in VESTA. Table S1 displays the lattice parameters of BVO. With the increment in the concentration of Er^{3+}, the lattice parameters decrease, leading to the conclusion that the Er^{3+} is substituting the Ba^{2+} site, since Er^{3+} is smaller than Ba^{2+}.

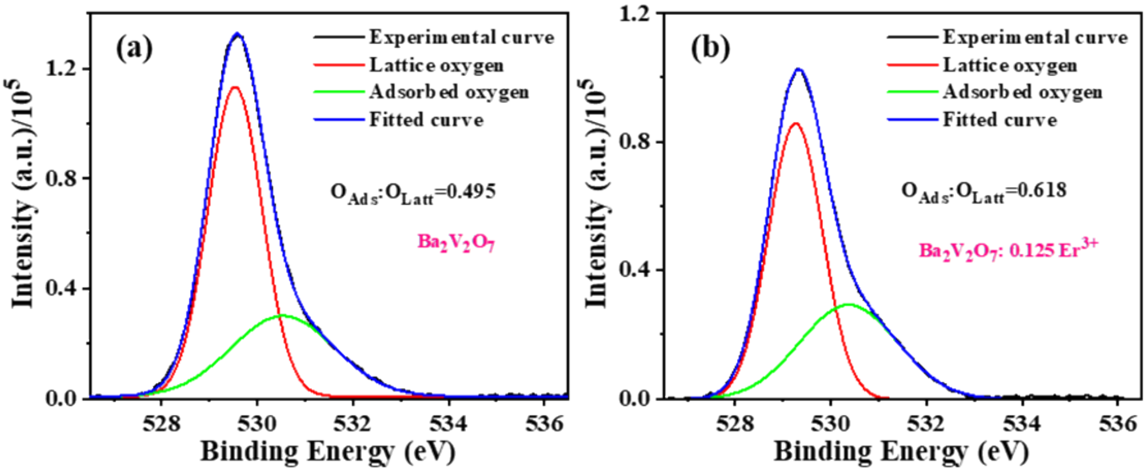

Fig. S2: High-resolution O1s XPS spectra of (a) undoped $Ba_2V_2O_7$ and (b) $Ba_2V_2O_7$: 0.125 Er^{3+}.

Fig. S2 shows the high-resolution O 1s spectra of the undoped $Ba_2V_2O_7$ sample and its doped counterpart, which show distinct multicomponent oxygen species. Accurate fitting was achieved by assuming two Gaussian peaks for the asymmetric O 1s peak. The lattice oxygen (O-M-O link) is responsible for the 529.5 eV peak, whereas the adsorbed oxygen (530.5 eV peak) is associated with the other peak, showing that both BVO and Er-doped BVO has oxygen vacancies. The ratio of adsorbed oxygen and lattice oxygen in Er-doped BVO is greater than that of pure BVO, indicating that the doped sample has a greater number of oxygen vacancies than the pure sample.

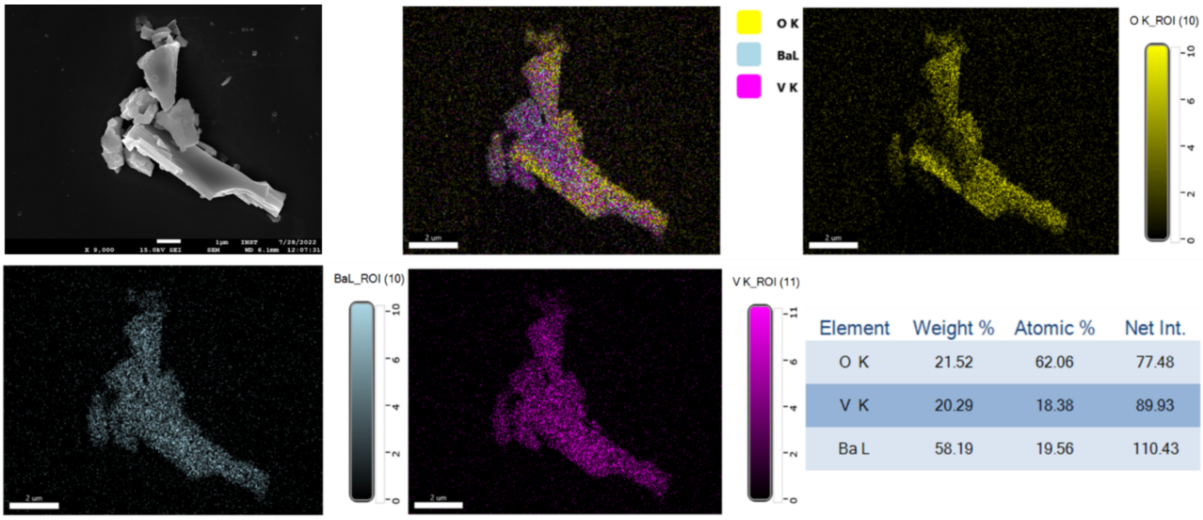

Element	Weight %	Atomic %	Net Int.
O K	21.52	62.06	77.48
V K	20.29	18.38	89.93
Ba L	58.19	19.56	110.43

Fig. S3 Elemental mapping of $Ba_2V_2O_7$ nanosheets.

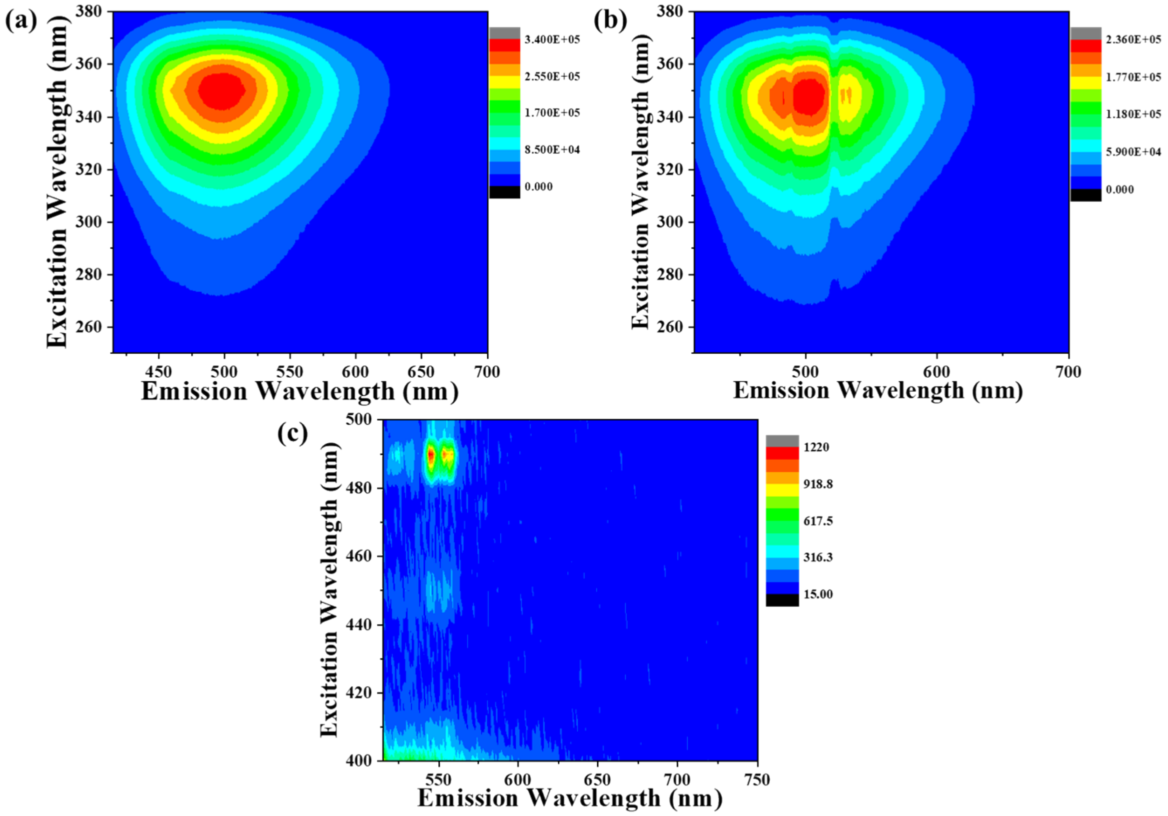

Fig. S4 Visible region emission-excitation contour plot of **(a)** undoped $Ba_2V_2O_7$, **(b)** and **(c)** $Ba_2V_2O_7$:0.125 Er^{3+}.

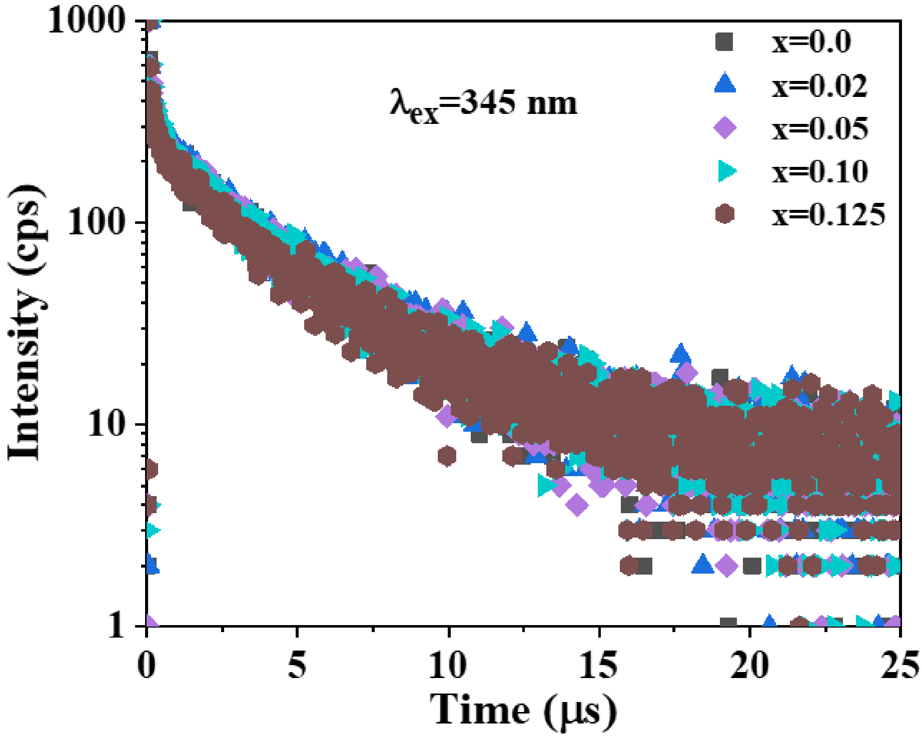

Fig. S5 Bi-exponential decay profile of Er^{3+} doped $Ba_2V_2O_7$ phosphor monitored under 345 nm excitation for 513 nm emission.

Table S2: Bi-exponential lifetime values of Er^{3+} doped $Ba_2V_2O_7$ phosphor (λ_{ex}= 345 nm, λ_{em}= 513 nm).

Concentration	**B_1**	**τ_1 (μs)**	**B_2**	**τ_2 (μs)**	**Average τ (μs)**
0.0	31.99	1.35	68.01	5.02	4.61
0.02	11.03	0.25	88.97	4.02	3.99
0.05	9.74	0.35	90.26	3.99	3.96
0.10	9.67	0.14	90.33	3.81	3.79
0.125	8.65	0.19	91.35	3.76	3.75

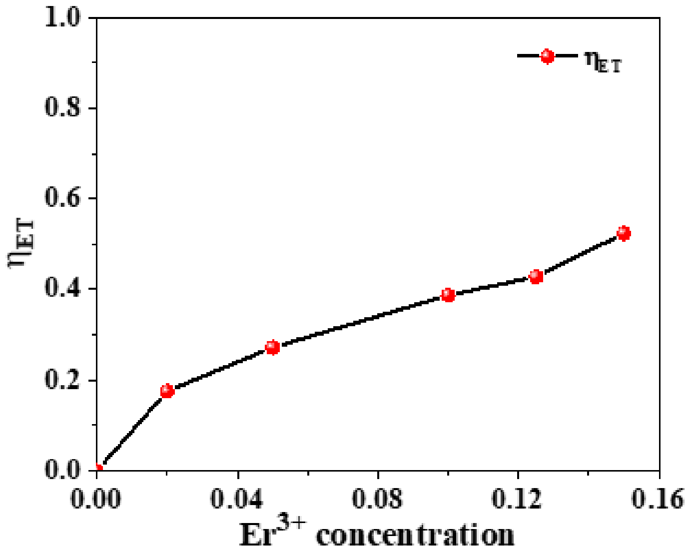

Fig. S6: Variation of energy transfer efficiency with Er^{3+} doping concentration.

The energy transfer efficiency (η_{ET}) is calculated from luminescence intensities using the following formula.

$$\eta_{ET} = 1 - \frac{I_S}{I_{S0}}$$

Where I_S signifies the integrated emission intensity of the donor in the presence of the activator. I_{S0} has the same meaning but in the absence of the activator.

The energy transfer efficiency of various Er^{3+} doped samples calculated from the absolute emission intensities is shown in Fig. S6. The energy transfer efficiency gradually increases to ~52% at BVO:0.15 Er^{3+}.

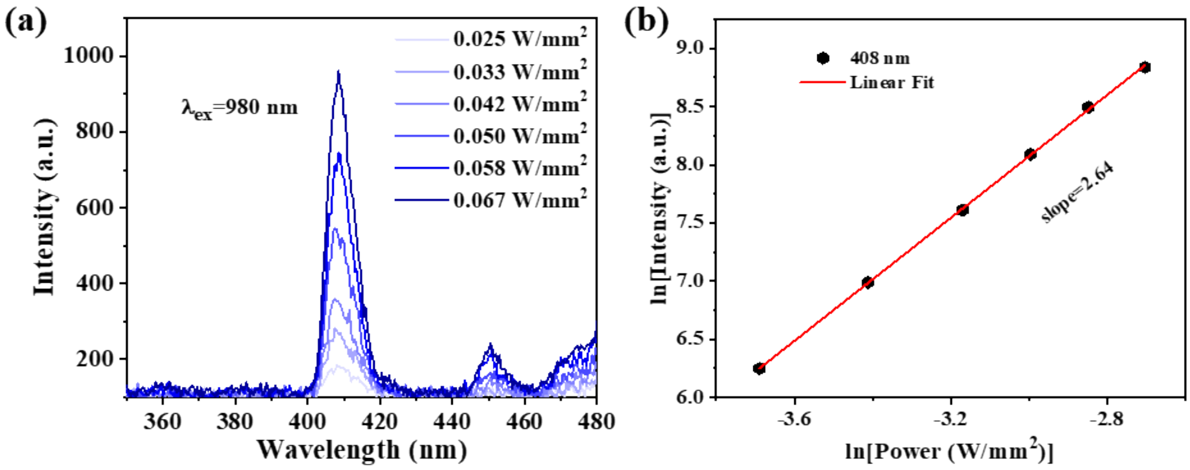

Fig. S7 (a) Pump power density dependent UC emission spectra and **(b)** logarithmic dependence of Intensity on Pump power density of Er^{3+} doped $Ba_2V_2O_7$ under 980nm LASER excitation.

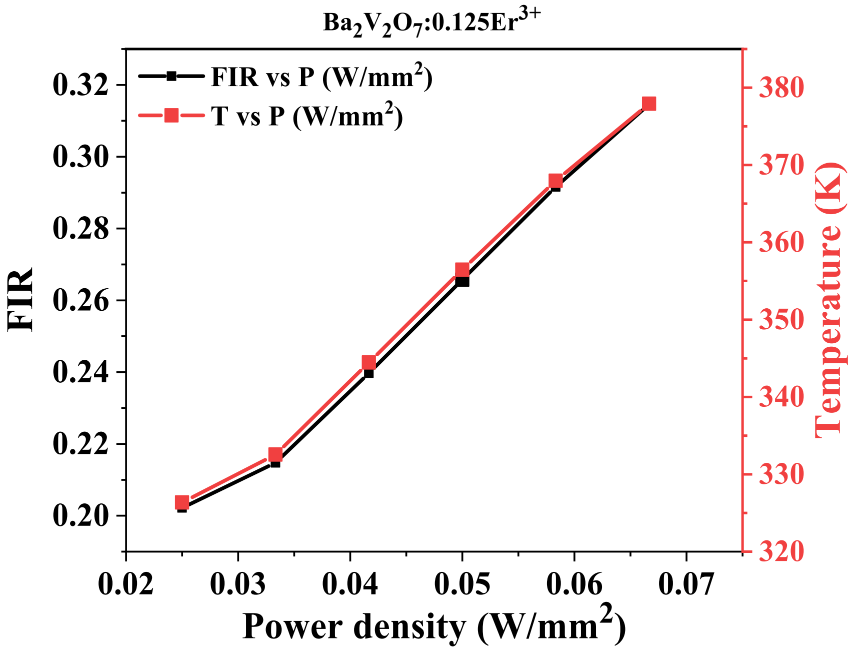

Fig. S8 Variation of FIR and temperature of BVO: 0.125Er^{3+} with various power densities under 980 nm excitation.

Some materials can convert laser energy to heat, raising the internal temperature. To quantify this, the FIR of BVO: 0.125Er^{3+} was plotted vs. pump power (Figure S8).

$$T = \left(\frac{\Delta E}{k_B}\right) \times \left(\frac{1}{\ln B - \ln FIR}\right) \tag{S1}$$

FIR values regularly rose from 0.20 to 0.31 with power. Based on optical temperature sensors, FIR values correlate to temperatures. Eq. (S1) shows how laser stimulation at different power densities affects sample temperature. Temperature rose monotonically from 326.6 to 377.9 K, while power densities rose from 0.025 to 0.067 W/mm^2. Based on the aforementioned findings, non-radiative relaxation (electron-phonon coupling) is crucial for induced heat in UC emission materials at increasing power densities, making them promising optical heaters for photothermal treatment. To reduce the optical heating caused by the laser, the thermometry measurements need to be done at the lowest pump power density which in this case would be 0.025 W/mm^2. If the measurement is done with different pump power densities, the laser heating correction should be applied, or a corresponding calibration curve needs to be used.

References:

1. F. C. Hawthorne, and C. Calvo*, J. Solid State Chem.*, 1978, **26**, 345-355.

2. S. Shi, D. Gao, Q. Xu, Z. Yang and D. Xue, *RSC Adv*, 2014, **4**, 45467–45472.